Numerical Model of Unsteady Subsonic Aeroelastic Behavior

Thomas W. Strganac*
NASA Langley Research Center, Hampton, Virginia
and
Dean T. Mook†
Virginia Polytechnic Institute and State University, Blacksburg, Virginia

The present paper describes a numerical simulation of unsteady subsonic aeroelastic responses. The technique accounts for aerodynamic nonlinearities associated with angles of attack, vortex-dominated flow, static deformations, and unsteady behavior. The fluid and the wing together are treated as a single dynamic system, and the equations of motion for the structure and flowfield are integrated simultaneously and interactively in the time domain. The method employs an iterative scheme based on a predictor-corrector technique. The aerodynamic loads are computed by the general unsteady vortex-lattice method and are determined simultaneously with the motion of the wing. Two models are used to demonstrate the technique: a rigid wing on an elastic support experiencing plunge and pitch about the elastic axis and an elastic wing rigidly supported at the root chord experiencing spanwise bending and twisting.

Nomenclature

A = wing reference area
$\{A\}$ = generalized aerodynamic loading vector
C = nondimensional aerodynamic constant = $\rho \ell_c A/2m$
C_α = nondimensional rotational damping = $c_\alpha/mU_\infty \ell_c$
C_m = aerodynamic pitch-moment coefficient
C_n = aerodynamic normal-force coefficient
C_y = nondimensional translational damping = $c_y \ell_c/mU_\infty$
c = chord
c_α = support rotational damping
c_y = support translational damping
EI = distributed bending stiffness
GJ = distributed torsional stiffness
g = acceleration due to gravity
I_e = mass moment of inertia referenced to the elastic axis
$[I]$ = identity matrix
K = nondimensional inertia = $I_e/m\ell_c^2$
K_α = nondimensional rotational stiffness = k_α/mU_∞^2
K_y = nondimensional translational stiffness = $k_y \ell_c^2/mU_\infty^2$
$[K]$ = stiffness matrix
k_α = support rotational stiffness
k_y = support translational stiffness
ℓ_c = characteristic length = c/n
M = distributed aerodynamic pitch moment
$[M]$ = mass matrix
m = mass or distributed mass
N = distributed aerodynamic normal force
n = number of chordwise (bound) lattice elements or number of first-order equations
q = generalized coordinates
r = distance between center of gravity (cg) and elastic axis (ea), positive for cg aft of ea
$\{S\}$ = static loading vector
T = period
U_∞ = freestream velocity
w = displacement of the elastic axis
x_α = local distance between the sectional elastic axis and center of gravity
$\bar{x}$ = distance between center of gravity (cg) and the aerodynamic reference, positive for cg aft of reference
Y = nondimensional plunge degree of freedom = y/ℓ_c
α = nondimensional pitch degree of freedom, or rotation about the elastic axis
η = time derivative of Y or the generalized velocities ($=\dot{q}$)
ξ = time derivative of α
ρ = density of fluid
Φ = bending or torsional free-vibration mode
ϕ = angle-of-attack of undeformed wing
$(\,)'$ = first derivative with respect to length
$(\,)''$ = second derivative with respect to length
$(\dot{u})$ = first derivative with respect to time (or nondimensional time)
$(\ddot{u})$ = second derivative with respect to time (or nondimensional time)
$(\,)_s$ = static component
$(\,)_d$ = dynamic component

Introduction

THE problem of modeling subsonic aeroelastic behavior is considered in the present paper. With the present model, the elastic structure and flowing air are considered a single dynamic system, and simulations of aeroelastic responses are obtained by integrating the equations of motion for both the fluid and the structure simultaneously and interactively, The simulations are not restricted by planform, twist, camber, or angle of attack, as long as the line of separation is known and vortex-bursting does not occur in the near flowfield. The present simulations are restricted to incompressible flows. The method is well suited for modeling vorticity-dominated flowfields.

The problem of two-dimensional flow over a rigid airfoil mounted on an elastic support has been receiving attention for many years. The first analyses considered incompressible flow and linear springs and are described in several excellent textbooks on aeroelasticity. About ten years ago, a significant advance was made when the analysis was extended to transonic flows. Because transonic flows are described by nonlinear equations, there were developed methods for numerically integrating simultaneously the governing equations for the flow and the dynamic equations of motion of the structure. The first efforts in this pioneering work were by Rizetta,[1,2] who also included a third degree of freedom for a flap, Ball-

Presented in part as Paper 87-0736 at the 28th Structures, Structural Dynamics and Materials Conference, Monterey, CA, April 6-8, 1987, and as Paper 87-1428 at the 19th Fluid Dynamics, Plasma Dynamics and Laser Conference, Honolulu, Hawaii, June 8-10, 1987; received Jan 4, 1988; revision received May 28, 1989.

*Research Engineer.
†Professor, Department of Engineering Science and Mechanics.

haus and Goorjian,[3] Yang, Guruswamy, and Striz,[4] Yang, Guruswamy, Striz, and Olsen,[5] and Guruswamy and Yang.[6] The work was the first to truly capture dynamic/aerodynamic interaction by considering the flowing fluid and airfoil together to be a single dynamic system.

Strganac[7] and Strganac and Mook[8] developed a method for analyzing the aeroelastic response of rigid finite-aspect-ratio wings mounted on elastic supports. The method is based on the general unsteady vortex-lattice method. The method is not restricted by aspect ratio or planform or curvature of the lifting surface, and it models the effects of the wing-tip vortex systems. Moreover, the method is not restricted by angle of attack as long as vortex bursting does not occur and separation occurs only along the edges of the lifting body. It is restricted to incompressible flow. The no-penetration boundary condition is imposed at the control points on the actual surface. The method can accommodate nonlinear structural models and small, but finite, amplitudes of the motion. Limit-cycle (i.e., postflutter) analyses are possible.

In addition to the efforts described above, there has been some attention given to the problem of modeling the aeroelastic response of flexible wings. Among the earliest investigators to capture dynamic/aerodynamic interaction by considering the wing and the flowing fluid to be a single dynamic system were Eastep and Olsen[9] and Borland and Rizzetta.[10] These efforts were directed toward transonic flows and used small-disturbance models of the flowfield. More recently, Strganac[7] and Strganac and Mook[11] also analyzed the unsteady aeroelastic behavior of flexible wing. As in their previous effort, the approach was not limited by aspect ratio, angle of attack, etc., but was restricted to subsonic flow.

Following a procedure that apparently was first proposed by Loring,[12] the investigators expressed the deflections as expansions in terms of the linear free-vibration modes and considered the time-dependent coefficients in these expansions to be the generalized coordinates of the motion. The aerodynamic loads were also expressed as expansions in the modes. Following Galerkin's procedure, they reduced the original set of governing partial differential equations to a finite set of ordinary differential equations. The ordinary differential equations were then integrated by essentially the same methods developed for rigid wings on elastic supports.

The technique described here provides an approach to the modeling of flutter for a wing of arbitrary planform. The governing equations are developed for motion about arbitrary static angles of attack, providing a new capability to study the associated nonlinear effects. Through the use of the unsteady vortex-lattice method (UVLM), one is able to treat low-aspect-ratio wings and account for the effect of the wake rollup at the wing tips. Moreover, the UVLM models the wake where the history of the motion resides. Because the governing equations are solved in the time domain, the method provides an opportunity to view the results through animation of the flowfield and wing motion.

Unsteady Vortex-lattice Method

The UVLM has been described in detail by Konstadinopoulos et al.,[13] so it is only briefly reviewed here. This numerical model of the three-dimensional flowfield can be used to treat arbitrary maneuvers of wings of arbitrary planforms, including highly swept delta wings which exhibit leading-edge separation, configurations of multiple closely coupled lifting surfaces, and low-aspect-ratio planforms. It can also treat arbitrary angles of attack and camber, as long as stall or vortex bursting in the near wake does not occur. The method accounts for the nonlinear effects of the wakes adjoining the tips and trailing edge. The ability of the UVLM to predict accurate spanwise distributions of static loads has been demonstrated previously.

The vortex lattice representation of a typical wing is illustrated in Fig. 1. The no-penetration condition is imposed at the control point of each element; two typical control points

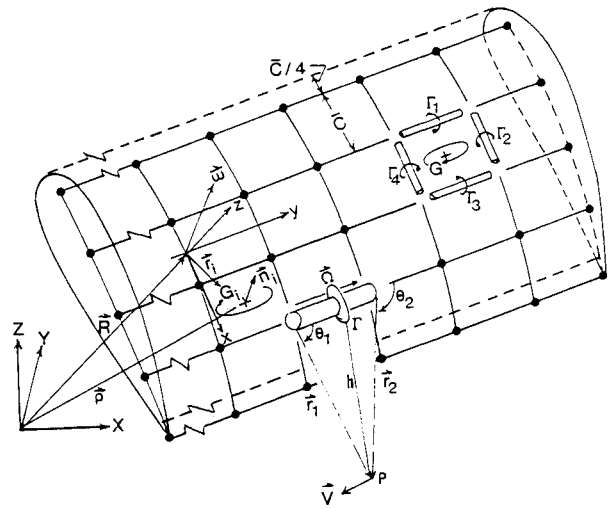

Fig. 1 A typical vortex lattice representing a lifting surface; the vortex segments are shown as solid lines, the intersections (called nodes) are shown as heavy dots, G is the circulation around a closed loop of four vortex segments, and Γ is the circulation around an individual element; the velocity field induced by a vortex segment is computed according to the Biot-Savart law: $V = [\Gamma/(4\pi h)](\cos\theta_1 - \cos\theta_2)\,[(\Omega x r_1)/(|\Omega x r_1|)]$.

are shown in the figure (denoted by small crosses). The intersections of the discrete lines in the lattice (called nodes) are represented by the heavy dots. Each element of area on the wing is surrounded by a closed loop of constant-circulation vortex segments. These segments join at the nodes, where the loops make sharp (typically 90 deg) turns.

The individual discrete vortex segments connecting the nodes are typically members of two different loops (the exceptions are the segments along the leading edge). Consequently, the circulation around an individual segment is the algebraic sum of the circulations around the two loops to which it belongs. In the figure, the Γ represent circulations around the individual segments, and the G represent circulation around the closed loops of segments.

The lattice of discrete lines serves as a computationally expedient imitation of the boundary layers on the lifting surface and the free shear layers in the wake. The velocity field induced by the vorticity is computed according to the Biot-Savart law (as shown in the figure); consequently, the velocity field satisfies the continuity equation and decays far from the wing and its wake.

The circulations around the loops (the G in the figure) are obtained from the no-penetration condition:

$$\sum_{j-1}^{N} A_{ij} G_j = (V_{LS} - V_W)_i \cdot n_i \qquad (1)$$

for $i = 1, 2, \ldots, N$. In Eq. (1), N is the number of elements chosen to represent the wings, A_{ij} is the normal component of the velocity at the control point of element i generated by a closed loop of unit circulation around element j, $(V_{LS} - V_W)_i$ are the velocity of the lifting surface and the velocity induced by the wake at the control point of element i, and n_i is the unit vector normal to the surface of element i. (The normal vectors are obtained from the cross products of the diagonals; the elements are not planar in general.)

The problem is posed in a moving reference frame; consequently, for a rigid wing the A_{ij} are constant. For an elastic wing, the A_{ij} must be computed at each time step.

To impose the Kutta condition (i.e., to make the jump in pressure across the lifting surface, ΔC_p, vanish along the tips and trailing edge), we convect the vorticity along the tips and trailing edge into the wake by displacing each node according to

$$\Delta r = v \Delta t \qquad (2)$$

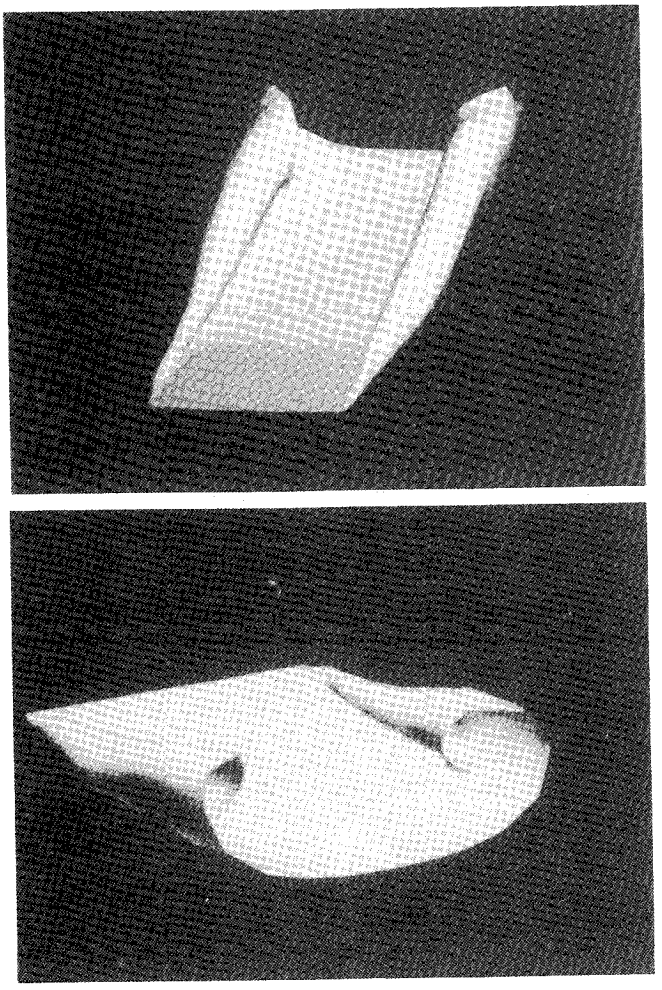

Fig. 2 Two different views of the vortex lattice representing a lifting surface and its wake, showing the rollup of the wing-tip vortex systems.

where Δr is the displacement of the node, v is the local velocity, and Δt is the time step. To maintain the wake in the force-free position, we also displace each node in the wake according to Eq. (2).

A flowfield predicted by the general UVLM is illustrated in Fig. 2. The wing and wake are modeled as a vortex lattice. The position of the portion representing the wing, commonly referred to as the bound vortex lattice, is specified, and, as a result, a finite pressure jump exists across it. The position of the portion representing the wake, commonly referred to as the free vortex lattice, is not specified; it is predicted as part of the solution. The elements depicted in the figure are triangular. A diagonal was added to the quadrilateral elements used in the computation to make the data compatible with the graphics software.

The aerodynamic loading is determined by calculating the pressure jump across the individual elements in the bound lattice. The pressure is calculated from Bernoulli's equation for unsteady flows.

The model has been nondimensionalized by defining a characteristic length ℓ_c and characteristic velocity U_∞. From these definitions, the characteristic time t_c is determined. It is desirable to have nearly uniform elements in the lattice. To achieve this, we chose the characteristic length to be the chord of the rectangular elements ($\bar{c}$ in Fig. 1). As a result, the streamwise lengths of the wake elements are approximately the same as the chordwise lengths of the bound elements when the dimensionless time step Δt is unity. With this scheme, an increase in the number of chordwise elements is accompanied by a corresponding decrease in the physical time step.

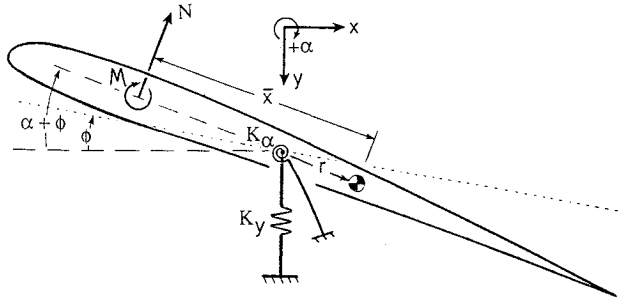

Fig. 3 A wing mounted on an elastic support. The aerodynamic force and moment are N and M, respectively; ϕ and α are the steady and unsteady portions of the angle of attack, respectively; K_α and K_y are the spring constants for pitch and plunge, respectively.

Equations of Motion of the Wings

Two structural models are used to demonstrate the procedure. The first model[7,8] is that of a rigid wing on an elastic support limited to plunge and pitch about the elastic axis. The second mode[7,11] is that of a flexible wing fixed at the root chord and introduces spanwise bending and twisting into the formulation. The general approach is not limited to these structural models but requires the set of first-order differential equations that represent the system of interest. Structural nonlinearities can be included. The UVLM is inherently nonlinear.

The equations of motion for the wing section illustrated in Fig. 3 were derived previously.[7,8] The nondimensional form of these equations can be written as

$$\ddot{Y}=\frac{1}{K-r^2\cos^2(\alpha+\phi)}\left[(C_\alpha\dot{\alpha}+K_\alpha\alpha)r\cos(\alpha+\phi)\right.$$
$$+K\dot{\alpha}^2 r\sin(\alpha+\phi)-K(C_y\dot{Y}+K_yY)$$
$$\left.-C\cos(\alpha+\phi)(nrC_m+KC_n)\right] \tag{3}$$

$$\ddot{\alpha}=\frac{1}{K-r^2\cos^2(\alpha+\phi)}\left[(C_y\dot{y}+K_yy)r\cos(\alpha+\phi)\right.$$
$$-R^2\dot{\alpha}^2\sin(\alpha+\phi)\cos(\alpha+\phi)-C_\alpha\dot{\alpha}-K_\alpha\alpha$$
$$\left.+C(nC_m+r\cos^2(\alpha+\phi)C_n)\right] \tag{4}$$

where the overdots represent derivatives with respect to nondimensional time, Y and α are the plunge and pitch coordinates, C_α and C_y are the damping coefficients for the support, K_α and K_y are the spring constants, ϕ is the static angle of attack, r is the distance between the elastic axis and the center of mass, C_n and C_m are the normal-force and pitch-moment coefficients, n is the number of elements in the chordwise direction, C is a dimensionless mass ratio and K a dimensionless moment-of-inertia ratio. In the nondimensional form, it is interesting to note that only the structural damping and stiffness coefficients are dependent upon the freestream velocity. As the velocity increases, the influence of damping and stiffness decreases.

The angle of attack for the wing in the static, undeformed position ϕ is introduced to permit the study of configurations at high angles of attack. The equations appear to be coupled only by r, the distance between the elastic axis and the sectional center of gravity; however, the aerodynamic loads C_n and C_m couple these equations because they depend upon α, $\dot{\alpha}$, and $\dot{y}$. In these equations the stiffness and damping are assumed to be linear; however, nonlinear structural properties may be introduced easily. Aerodynamic nonlinearities are modeled by the UVLM.

The equations of motion for a wing with bending and twisting,[7,11] such as the one illustrated in Fig. 4, also were

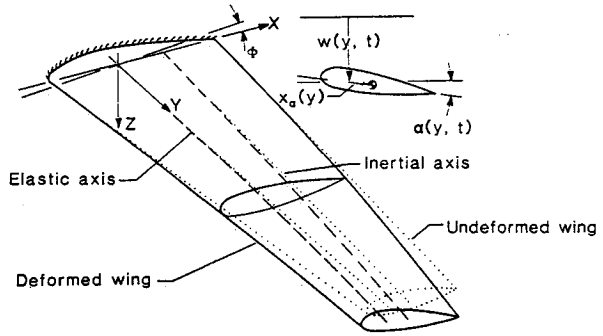

Fig. 4 A schematic drawing of an elastic wing cantilevered at its root chord.

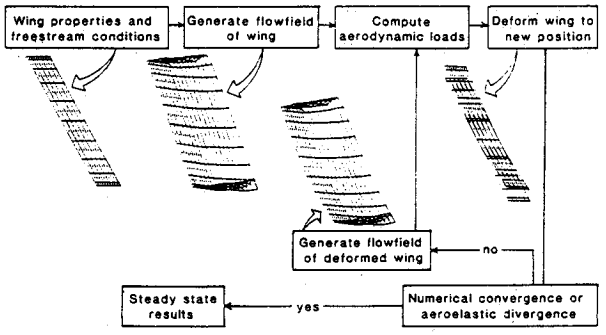

Fig. 5 Flow chart describing the method of solution for the static deformations.

derived previously. These equations are

$$(Elw_s'')'' - mg = -N_s \tag{5a}$$

$$-(GJ\alpha_s')' - mgx_\alpha = M_s \tag{5b}$$

$$m\ddot{w}_d + mx_\alpha\ddot{\alpha}_d + (Elw'')'' = -N_d \tag{6a}$$

$$I_e\ddot{\alpha}_d + mx_\alpha\ddot{w}_d - (GJ\alpha_d')' = M_d \tag{6b}$$

where primes denote partial derivatives with respect to y (the spanwise coordinate), overdots denote partial derivatives with respect to time, EI and GJ are the bending and torsional stiffnesses, w_s, w_d and α_s, α_d are the static and dynamic components of the deflection, m is mass per unit of length, g is gravitational acceleration, N_s, N_d, M_s, and M_d are static and dynamic normal-force and pitch-moment loads, I_e is the mass moment of inertia, and x_α is the distance between the elastic and inertial axes. The boundary conditions for this formulation are representative of a cantilevered wing.

The solution of this set of equations provides both the static and dynamic contributions. The aerodynamic spanwise loading, which is provided by the UVLM, depends on the static deformations, motion, and geometry. The dependent variables w and α are represented by expansions in terms of the free-vibration modes of the system, Φ_j:

$$w = \sum_{i=1}^{I} q_i\Phi_i \text{ and } \alpha = \sum_{J=I+1}^{J} q_j\Phi_j \tag{7}$$

where I is the number of flexural modes selected and $J - I$ is the number of torsional modes. The time-dependent coefficients in these expansions, $q_j(t)$, are separated into static and dynamic contributions:

$$\{q\} = \{q_s\} + \{q_d\} \tag{8}$$

Substituting Eqs. (7) and (8) into Eqs. (5) and (6) and following Galerkin's procedure leads to a set of equations of the following form:

$$\{q_s\} = [K]^{-1}\{\{A_s\} + \{S\}\} \tag{9}$$

and

$$\{\ddot{q}_d\} = -[M]^{-1}\{[K]\{q_d\} + \{A_d\}\} \tag{10}$$

where $\{A_s\}$ and $\{A_d\}$ are the steady and unsteady parts of the aerodynamic loading (expanded in terms of the modes) and $\{S\}$ is the load due to gravity. $\{A_d\}$ is a function of the static load.

Initially the static solution is found. Then the dynamic equations are written as a system of $2J$ first-order equations of the form

$$\begin{Bmatrix}\{\dot{\eta}\}\\ \{\dot{q}_d\}\end{Bmatrix} = \begin{bmatrix}[0] & -[M]^{-1}[K]\\ [I] & [0]\end{bmatrix}\begin{Bmatrix}\{\eta\}\\ \{q_d\}\end{Bmatrix} + \begin{Bmatrix}[M]^{-1}\{A_d\}\\ \{0\}\end{Bmatrix} \tag{11}$$

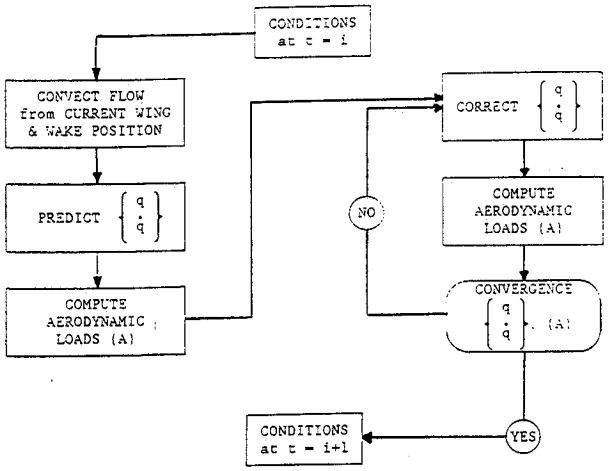

Fig. 6 Flow chart describing the method of solution for the unsteady deformations.

Numerical Integration Scheme

For the elastic wing, the static solution is obtained prior to the start of the dynamic solution. The procedure for the static wing is illustrated in Fig. 5. The analysis of the static problem begins with the calculation of the distributed loads on the undeflected wing. These loads are used to calculate the bending and torsional deflections. At this point the wing has a new shape, but the loads still correspond to the old shape. New loads, corresponding to the new shape, are obtained next; then the corresponding new shape is obtained. The procedure is repeated until both the shape and loads converge or aeroelastic divergence occurs. The elements with dots at their centroids are part of the bound lattice (wing); the others are part of the free lattice (wake). In Fig. 5, the wing is represented in both its deformed and undeformed shapes.

The interaction between the aerodynamic loads and wing motion presents an interesting challenge: the loads are necessary to predict the motion, and the motion is necessary to predict the loads. The integration technique for the dynamic solution is illustrated in the flowchart of Fig. 6. The solution for the rigid wing on an elastic support is computed in a similar way.

Numerical Results

The technique is demonstrated for both the rigid wing and on an elastic support and the elastic wing.

In Fig. 7, the vertical and angular displacements of the rigid wing on an elastic support are shown as functions of time. The dynamic pressure is above the critical value, and the motion

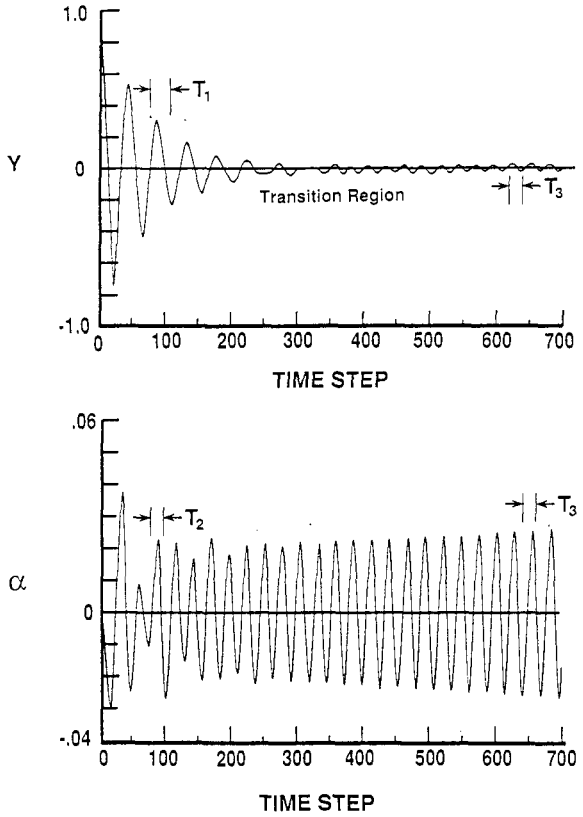

Fig. 7 Plunge (Y) and pitch (α) as functions of time for a rigid wing mounted on an elastic support; the airspeed is above the critical; the periods of the two motions change from T_1 and T_2 to a common value T_3.

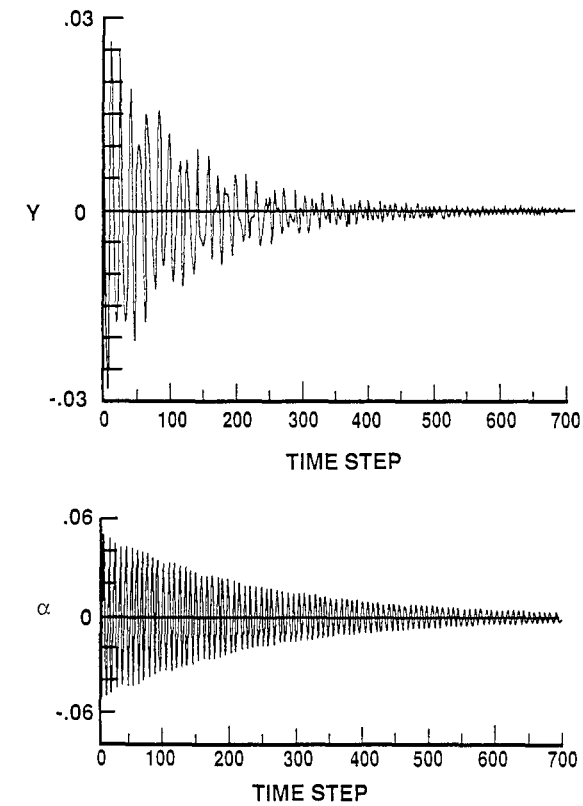

Fig. 8 Plunge (Y) and pitch (α) as functions of time for a rigid wing mounted on an elastic support; the airspeed is below the critical; there is no transition to a common period.

was started by a large initial vertical displacement. Initially, the linear and angular motions have different periods (T_1 and T_2 in the figure), which are nearly the periods for the individual one-degree-of-freedom free vibrations. Around time step 200, both the vertical and angular motions begin to experience a change in period. The change is more evident in the time record of the vertical motion. By time step 500, both motions have the same period (T_3 in the figure). Note that T_3 is noticeably smaller than T_1 and slightly larger than T_2. The motions appear to be growing slowly toward a limit cycle; clearly, they are not experiencing exponential growth. The growth is limited by the aerodynamic model, which is inherently nonlinear. The springs are linear.

In Fig. 8, the vertical and angular motions are shown as functions of time when the dynamic pressure is below the critical value. The motions clearly decay to the static equilibrium positions, and no transition to a common frequency occurs.

Next, we illustrate the response of an elastic wing for dynamic pressures below and above the flutter boundary. The physical characteristics of this example are specified in Ref. 7. The natural free-vibration modes may be obtained by any

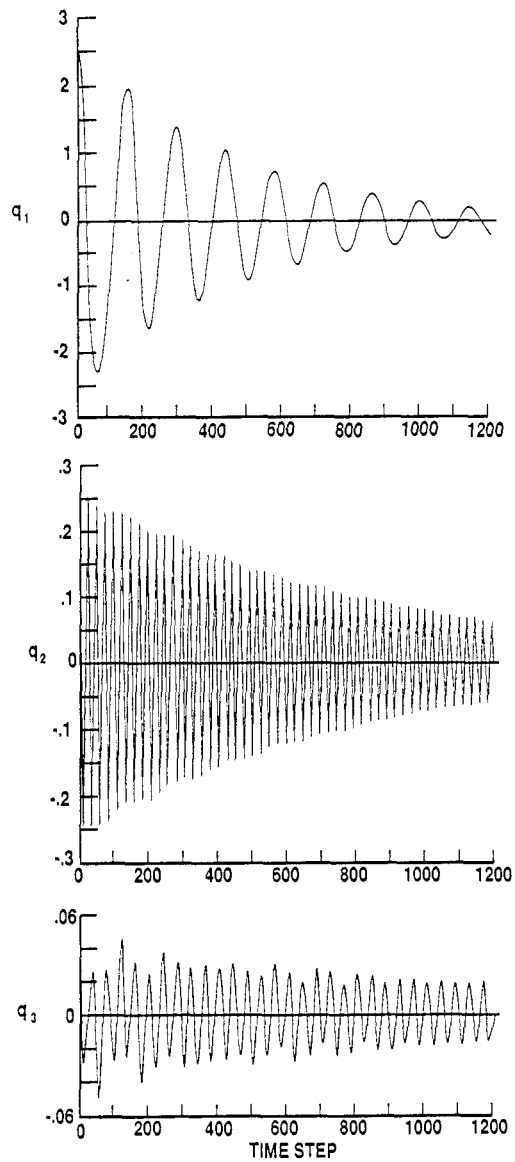

Fig. 9 Modal amplitudes for a flexible wing cantilevered at the root chord as functions of time; q_1, q_2, and q_3 are the amplitudes of the first and second bending modes and the first torsional mode, respectively; the airspeed is below the critical.

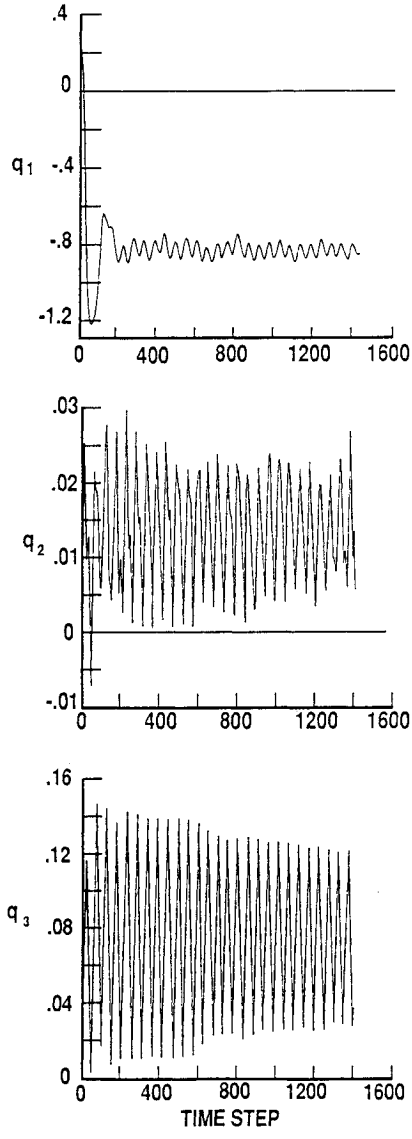

Fig. 10 Modal amplitudes for a flexible wing cantilevered at the root chord as functions of time; q_1, q_2, and q_3 are the amplitudes of the first and second bending modes and the first torsional mode, respectively; the airspeed is above the critical.

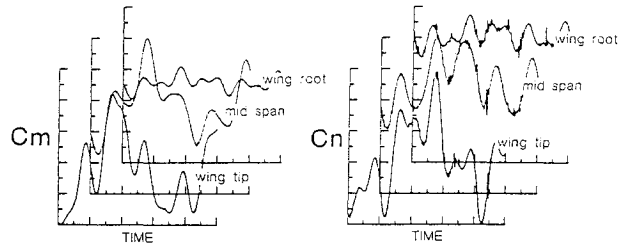

Fig. 11 Sectional pitch-moment (c_m) and normal-force (c_n) coefficients as functions of time for different spanwise positions.

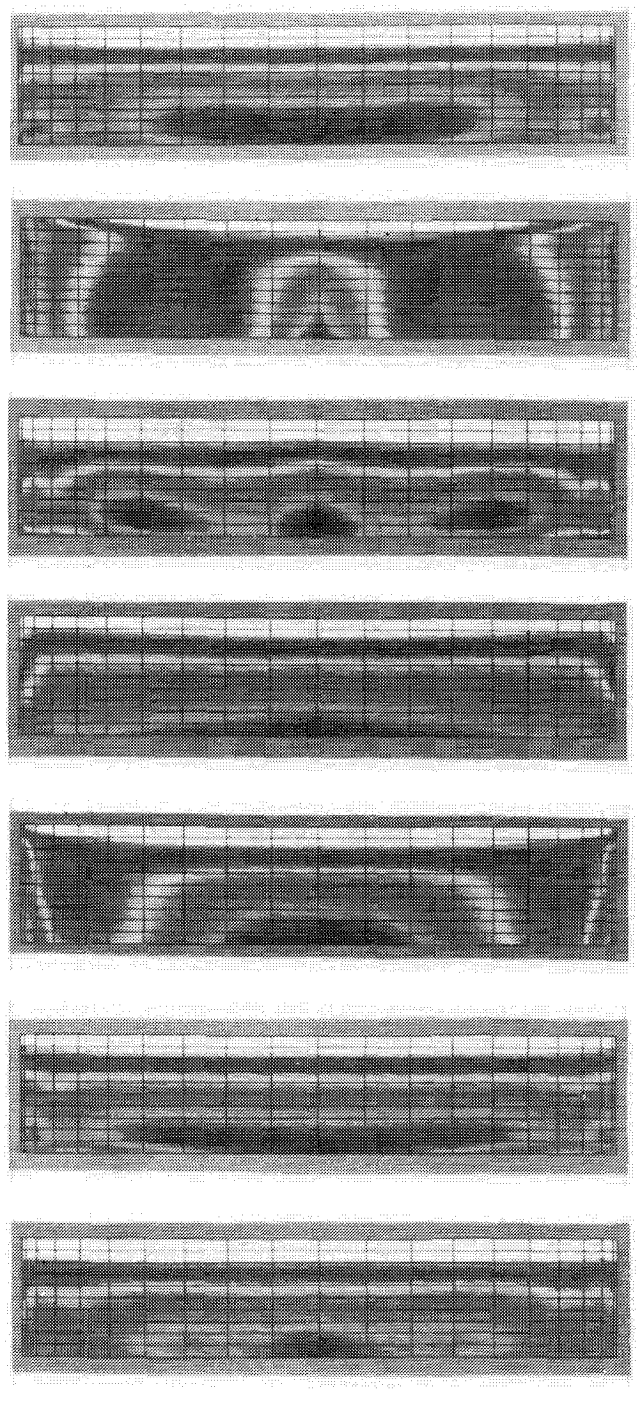

Fig. 12 Vorticity and loading intensity distributions for seven different times in the cycle of the motion depicted in Fig. 13; light regions are highly loaded.

available means. We used a finite-difference scheme to solve the two-point boundary-value problem. The deformations of the wing are represented by the first two bending modes and the first torsional mode. The natural frequencies, scaled to the first bending mode, are 1.0, 5.91, and 4.55 for the two bending modes and the torsional mode, respectively.

In Fig. 9, the dynamic parts of the amplitudes of the three modes are shown as functions of time. The dynamic pressure is below the critical value, and the initial disturbance is a relatively large displacement in the first bending mode only. The motion apparently decays. The periods of the three functions are different and near those for the free vibrations of the individual modes.

In Fig. 10, the dynamic parts of the three modal amplitudes are shown as functions of time, when the dynamic pressure is above the critical value. The periods of the individual modal coefficients begin to change around time step 200. After time step 400, the periods for all three are the same, in contrast with the response shown in Fig. 9. Moreover, the motion is not around the static equilibrium position; a drift occurs. The mean deflection in the first bending mode decreases, whereas the means of the second mode and the torsion mode increase.

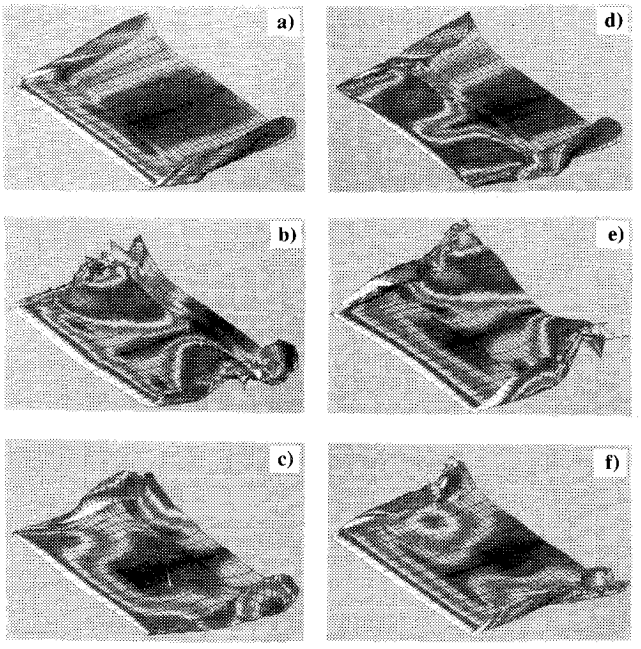

Fig. 13 A sequence of views showing the flexible wing and its wake at different times in the cycle; light colors indicate regions of intense vorticity.

Drift is a common nonlinear phenomenon. In the present example, the structure is governed by linear equations, but the aerodynamic model is inherently nonlinear.

In Fig. 11, the sectional normal-force and pitch-moment coefficients are shown as functions of time at three spanwise locations. The peaks are much greater near the wing tip where the motion is larger. Moreover, the peaks do not occur at the same time at all stations, and the present method permits one to obtain the phases among them.

In Fig. 12, the vorticity distribution on the lifting surface is shown for seven different positions through the cycle. The light regions are regions of intense vorticity concentrations and, hence, regions of large pressure difference, high loading. As one would expect, the pressure difference is greatest at the leading edge. The patterns reveal how the pressure distribution varies with the motion. The motion considered is symmetric with respect to the midspan chord. Symmetry was imposed in the present solution, but is not an essential feature of the method. In several parts of the figure, one can see strong pressure differences near the wing tips (see, e.g., part e). The nearly chordwise line of high-pressure difference is caused by the strong wing-tip vortex that develops during the downward motion of the wing tips. Wing-tip vortex systems are predicted by the present simulation.

The predicted motions of the wing and wake can be animated. In Fig. 13, a sequence of representative frames from a movie are shown. The first picture shows the wing and wake immediately following the initial disturbance. The deformations include contributions from both static and dynamic loads. The intensity of vorticity as it varies spatially in the wing and wake is also shown. In part b, the system is represented shortly after the initial disturbance has started to convect downstream. The remaining parts of this sequence show the wing and wake at subsequent positions during the motion. The geometry of the wing and wake continue to change. It is interesting to note that the wing-tip vortex system breaks down and reforms with the bending/torsion motion. The loads that are used to calculate the motion reflect this behavior. The history of the motion is embedded in the wake.

Concluding Remarks

A method for predicting the steady and unsteady aeroelastic behavior of a wing has been described. The equations governing the motion of the structure are coupled with the equations governing the motion of the fluid, and the fluid and structure are treated as a single dynamic system. The partial differential equations governing flexible wings are reduced to a set of ordinary differential equations by Galerkin's method. The set of ordinary differential equations is integrated by a predictor-corrector algorithm. The results predict simultaneously and interactively the motion of the structure and the fluid in the time domain. The wake is generated as part of the solution; hence, the history of the motion is included in the technique. The method can be used to predict steady-state static responses and transient responses to initial disturbances.

The rigid-wing model accounts for the nonlinear effects of static angles of attack and finite aspect ratios and can be easily extended to demonstrate nonlinear structural behavior in the elastic support. Currently, the model of the elastic wing treats the nonlinear effects of the static angle of attack, but is limited by linear governing equations for the structure. However, the present approach can be readily extended to solve nonlinear equations governing large deformations of the structure.

References

[1]Rizetta, D. P., "Time-Dependent Responses of a Two-Dimensional Airfoil in Transonic Flow," *AIAA Journal,* Vol. 17, No. 1, 1979, pp. 26–32.

[2]Rizetta, D. P., "Transonic Flutter Analysis of a Two-Dimensional Airfoil," AFFDL, TM-77-64-FBR, 1977.

[3]Ballhaus, W. F., and Goorjian, P. M., "Computation of Unsteady Transonic Flows by the Indicial Method," *AIAA Journal,* Vol. 16, No. 2, 1978, pp. 117–124.

[4]Yang, T. Y., Guruswamy, P., and Striz, A. G., "Aeroelastic Response Analysis of Two-Dimensional, Single and Two Degree of Freedom Airfoils in Low Frequency, Small Disturbance Unsteady Transonic Flow," AFFDL, TR-79-3077, 1979.

[5]Yang, T. Y., Guruswamy, P., Striz, A. G., and Olsen, J. J., "Flutter Analysis of a NACA 64A006 Airfoil in Small Disturbance Transonic Flow," *Journal of Aircraft,* Vol. 17, No. 4, 1980, pp. 225–232.

[6]Guruswamy, P., and Yang, T. Y., "Aeroelastic Time Response Analysis of Thin Airfoils by Transonic Code LTRAN2," *Computers and Fluids,* Vol. 9, No. 4, 1981, pp. 409–425.

[7]Strganac, T. W., "A Numerical Model of Unsteady Subsonic Aeroelastic Behavior," Ph.D. Thesis, Dept. of Engineering Science and Mechanics, Virginia Polytechnic Inst. and State Univ., Blacksburg, VA, Aug. 1987.

[8]Strganac, T. W., and Mook, D. T., "Application of the Vortex-Lattice Method to the Nonlinear Two-Degree-of-Freedom Aeroelastic Problem," AIAA Paper 86-0867, 27th Structures, Structural Dynamics and Materials Conference, May 1986.

[9]Eastep, F. E., and Olsen, J. J., "Transonic Flutter Analysis of a Rectangular Wing with Conventional Airfoil Sections," *AIAA Journal,* Vol. 18, No. 10, 1980, pp. 1159–1164.

[10]Borland C. J., and Rizzetta, D. P., "Nonlinear Transonic Flutter Analysis," *AIAA Journal,* Vol. 20, Nov. 1982, pp. 1606–1615.

[11]Strganac, T. W., and Mook, D. T., "A New Method to Predict Unsteady Aeroelastic Behavior," AIAA Paper 87-0736, 28th Structures, Structural Dynamics and Materials Conference, April 1987.

[12]Loring, S. J., "General Approach to the Flutter Problem," SAE Transactions, Vol. 49, No. 2, 1941, pp. 345–356.

[13]Konstadinopoulos, P. A., "Numerical Simulation of the Subsonic Wing-Rock Phenomenon," Ph.D. Thesis, Dept. of Engineering Science and Mechanics, Virginia Polytechnic Inst. and State Univ., Blacksburg, VA, March 1984.